

## Operational window for the modified ITER divertor

A.S. Kukushkin<sup>1</sup>, H.D. Pacher<sup>2</sup>,

V. Kotov<sup>3</sup>, G.W. Pacher<sup>4</sup>, D. Reiter<sup>3</sup>

<sup>1</sup> ITER Organization, Cadarache, France; <sup>2</sup> INRS-EMT, Varennes, Québec, Canada;

<sup>3</sup> FZ Jülich, Jülich, Germany; <sup>4</sup> Hydro-Québec, Varennes, Québec, Canada

The modification of the divertor design developed in the course of the ITER design review has been integrated into the ITER baseline for the initial, non-active stage of machine operation. This new design provides more freedom for plasma positioning, thus relaxing the requirements on the equilibrium control system, and expands the operating space in terms of plasma self-inductance and poloidal flux state. Although divertor replacement is presently foreseen before the start of D operation, the design of the first divertor should not preclude its use during initial tritium experiments. Performance analysis for this divertor must therefore cover both the non-fusion, low-activation phase (H and He plasma operation) and full-scale operation with fusion power release. First SOLPS (B2-Eirene) simulations of this new design [1] find that the divertor continues to satisfy the criteria of target power loading and helium removal efficiency for the standard ITER burning plasma scenario ( $Q_{DT} = 10$ ). Work is ongoing to expand this earlier analysis in order to develop improved scalings of the plasma parameters at the interface to the plasma core in this new geometry, which, when used as the boundary conditions for the core plasma, permit efficient coupling the core and edge plasma models for the exploration of the ITER operational space [2]. An exploration of variations of the input power to the SOL in these simulations shows that acceptable operational regimes can be found at higher power,  $P_{SOL} = 120$  MW (compared with the 100 MW expected for  $Q_{DT} = 10$  operation). The results of [1] thus have some margin in terms of input power.

The new divertor design is such that magnetic equilibria are now possible which are less constrained by wall and divertor baffle elements and correspond to a wider SOL grid. To discriminate between the effects of changes in the divertor geometry and the width of the SOL modelled, a dedicated series of code runs

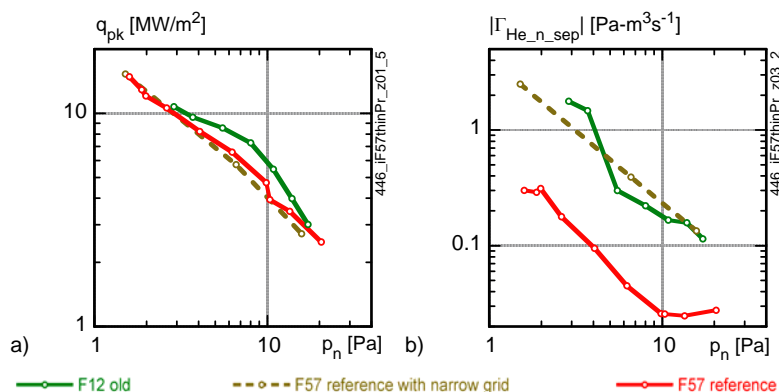


Fig. 1. The peak power (a) and the He atom influx to the core (b) vs. neutral pressure in PFR for the old divertor geometry, the new one, and for the new design with the narrow grid variant

has been performed in which a narrow grid (4 cm SOL width at the outer mid-plane, as in old geometry, compared with 9 cm for the new configuration), built with the new equilibrium, has been used in conjunction with the new design. This study confirms the conclusion in [1]

that at the same neutral pressure at the entrance to the pump duct,  $p_n$ , the detachment behaviour is somewhat modified (the peak temperature at the inner divertor falls at lower  $p_n$ ), but the peak power does not change and the drastic reduction of the neutral influx to the core is indeed due to the wider SOL of the new magnetic configuration, Fig. 1.

Scenarios for the low activation phase which will precede DT operation rely strongly on helium discharges, attractive because of their expected lower power threshold for H-mode access relative to hydrogen discharges. They should provide an opportunity for ITER to operate in H-mode with discharges at half plasma current and toroidal magnetic field (7.5 MA, 2.45 T) and thus test ELM mitigation techniques in the non-active, lower power phase. Since direct He fuelling is not presently available in the ITER baseline (there are no He pellets and the neutral beam injectors are currently not designed to work with He), core He fuelling relies on He atom penetration through the SOL and the modifications of the core He profile that could be provided by an anomalous pinch (see discussion in [3]).

For the first series of simulations, we have chosen to investigate the (more complex) He scenario in which ELM control by pace-making with H pellets is tested, implying significant core H fuelling in addition to a small contribution from heating beams. The plasma is assumed to consist of He, H, Be, and C ions and neutrals (corresponding to CFC vertical divertor targets which are to be used during the non-active phases). Helium is intended to be the major component; it is supplied by gas puffing from the top of the poloidal cross-section with no core He fuelling. Core H fuelling is simulated as a constant ion flux from the core of  $5 \cdot 10^{21}$  ions/s ( $\sim 9 \text{ Pa} \cdot \text{m}^3/\text{s}$ ). Be and C are produced through physical (both by He and H) and chemical (only C by H) sputtering of the first wall and targets, respectively. He and H are exhausted through the pump duct located under the dome, and Be and C are absorbed at every surface. The radial transport coefficients for all species are taken to be identical to those used for the D-T plasma simulations ( $D_{\perp} = 0.3 \text{ m}^2/\text{s}$  and  $\chi_{\perp} = 1 \text{ m}^2/\text{s}$ ). Re-erosion of deposits and material mixing are not considered here. The power input to the SOL from the core is 60 MW (compared with the 100 MW used for the DT simulations), corresponding to the full heating power assumed to be available for He plasmas (73 MW) minus 20% core radiation. The simulations were done with a pumping speed a factor 2.5 lower than that used for DT runs. We do not yet have enough data for He to perform the type of scaling of the edge plasma parameters reported in [4]. The comparison between He and DT performance is therefore performed in terms of dependence on  $p_n$  (including all neutral species).

These first runs show immediately that the detachment state in He is unclear. Two indicators for detachment are contradictory, i.e. the maximum temperature at the inner divertor falls at higher  $p_n$  for He than for DT, whereas the ion saturation current,  $I_{sat}$  rolls over at lower  $p_n$ . The peak power load,  $q_{pk}$ , is lower at the same  $p_n$  and  $P_{SOL}$  for He plasma, Fig. 2a, but would be similar at the same  $p_n$  to the DT case when the latter is scaled to the same  $P_{SOL}$  and pumping speed  $S_p$  using a scaling similar to that of [4] based on recent DT simulations. An important observation is that at low  $p_n$ , the target loading can be comparable

to that predicted for DT operation, thus allowing commissioning of high-heat-flux components (HHFC) in the divertor already in the non-active phase. Once  $q_{pk}$  goes below  $4 \text{ MW/m}^2$ , the maximum peak power shifts from the outer to the inner target for both He and DT operation – the in-out asymmetry of target loading is about the same. Despite the high H fraction (see later), He still dominates the radiation except at the low  $p_n$ , high  $q_{pk}$  end of the range, Fig. 2c.

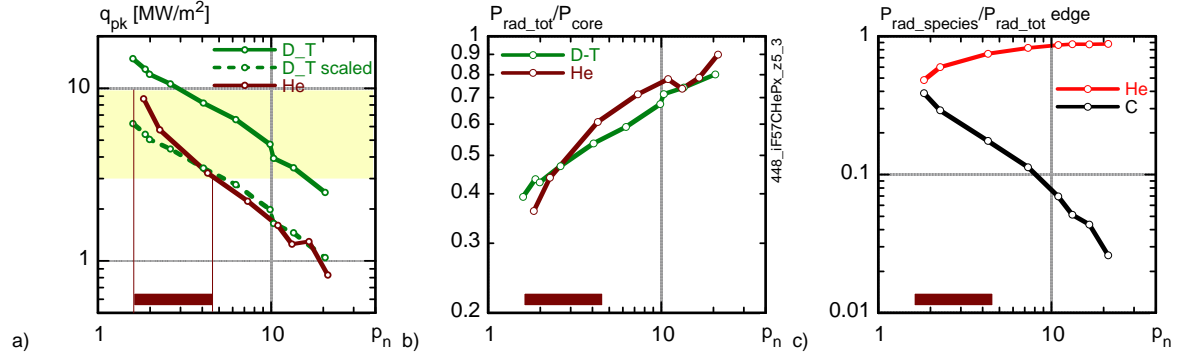


Fig. 2. Peak power load (a), total radiation fraction in the edge (b), and relative fraction of power radiated by He and C ions in He plasma (c) vs. neutral pressure at the entrance to the PFR [Pa] for DT and He operation. DT data scaled to the He power and pumping speed are shown with dashed line in (a). Horizontal bar shows pressure range for  $3 < q_{pk} < 10 \text{ MW/m}^2$  in He.

The operational window for HHFC commissioning experiments extends from the maximum acceptable loading of the targets ( $10 \text{ MW/m}^2$ ) to the minimum relevant loading – say,  $3 \text{ MW/m}^2$  (in the simulations, then  $\sim 60\%$  power entering the SOL is radiated). In this range, for the reduced power and pumping speed of this He operation, the He throughput varies from 1 to  $10 \text{ Pa}\cdot\text{m}^3/\text{s}$  and produces a separatrix electron density of  $2.2 \cdot 10^{19} \text{ m}^{-3}$ . This is about a factor 2 lower than in DT operation and compatible with the 7.5 MA/2.45 T scenario considered for He plasma operation in ITER [3] but lower than the shine-through limit of  $3 \cdot 10^{19} \text{ m}^{-3}$  given in [3]. At the pump duct, the neutral He pressure in this range of  $q_{pk}$  is in the range 0.2 to 2 Pa, Fig. 3a. It is much lower than the DT pressure predicted for full power DT operation at low  $p_n$  because of the rather high H content in the pumped gas ( $p_n$  includes H pressure) under these particular conditions, Fig. 3c. The core fuelling by neutrals is higher for He at the same  $p_n$ , Fig. 3b, and even much higher relative to the throughput – the SOL is much less opaque for He. However, only about  $4 \text{ Pa}\cdot\text{m}^3/\text{s}$  ( $10^{21}$  at/s) of core fuelling result from this flux within the  $q_{pk}$  range. A rough estimate shows that this would be marginally sufficient to sustain the minimum core He density of  $1.5 \cdot 10^{19} \text{ m}^{-3}$  ( $1/2 n_e$ ) required to prevent beam shine-through [3] if, taking a plasma surface area of  $700 \text{ m}^2$  and a pedestal width of 0.1 m, the He ion diffusivity in the pedestal were  $\leq 0.03 \text{ m}^2/\text{s}$ .

The strong H influx used as input in these modelling runs leads to a considerable He dilution in the edge. Fig. 3c shows different estimates for the relative concentration of H in the H – He mix, showing that it decreases as  $p_n$  is increased by increasing the He puffing rate. At low  $p_n$ , this concentration is highest in the pumped flux and the core fuelling (which is equal to the ion outflux from the core in steady state in the absence of core sinks), and lowest

in the neutral influx to the core – the SOL opacity for H neutrals is higher than for He. The H concentration in the ion density changes little at the separatrix. Since 3-body recombination of He ions is not included in the model (no data available), H recombination may be responsible for the drop of the  $I_{sat}$  on the targets seen in the calculations.

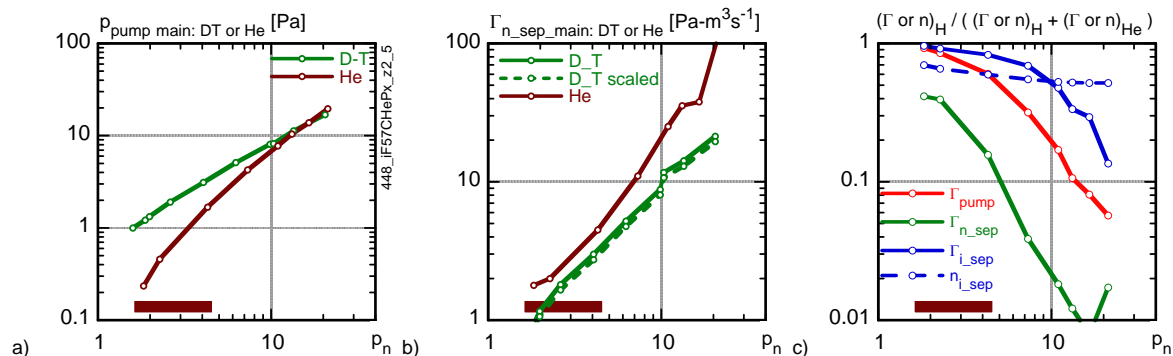


Fig. 3. Dependence on  $p_n$  of neutral pressure at the pump duct (a), neutral influx to the core (b) for DT and He operation and different estimates of H fraction in H-He mix in the He operation (c). DT data scaled to the He power and pumping speed are shown by the dashed line in (b). See also Fig. 2.

For the region of operating space over which the H fraction in the core in stationary conditions would significantly increase the H-mode threshold over that expected for pure He operation, useful tests of ELM H pellet pace-making could still be performed transiently, beginning with only minor contamination by the H beams. The H from pellet injection would only accumulate in several seconds, allowing a significant number of induced ELMs with majority He plasma.

Therefore, the initial SOLPS modelling results for He plasma operation with H fuelling due to pellet pace-making indicate that operation with target loading in the same range as that expected during DT operation may be achievable under non-active conditions, allowing commissioning of high heat flux components in the divertor. He gas puffing appears marginally sufficient to sustain a plasma density in the core required to avoid excessive beam shine-through loads on the first wall, relying on a combination of low pedestal diffusivity, lower power, and some anomalous inward pinch for He ions. The He dilution with H can be rather high in the edge plasma in these conditions, but in the power balance He radiation is still larger than that of H-produced C. More studies on He plasma, including exploration of the parameter space for the edge plasma, consistent core-edge modelling, model validation against experimental data, and refinement of the atomic data for helium are needed to support the initial phase of ITER.

This report was prepared as an account of work by or for the ITER Organisation. The Members of the Organisation are the People's Republic of China, the European Atomic Energy Community, the Republic of India, Japan, the Republic of Korea, the Russian Federation, and the United States of America. The views and opinions expressed herein do not necessarily reflect those of the Members or any agency thereof. Dissemination of the information in this paper is governed by the applicable terms of the ITER Joint Implementation Agreement.

- [1] A.S. Kukushkin, H.D. Pacher, A. Loarte, et al., *Nucl. Fusion* **49** (2009) 075008
- [2] G.W. Pacher, H.D. Pacher, G. Janeschitz, A.S. Kukushkin, *Nucl. Fusion* **48** (2008) 105003
- [3] A. Polevoi, D. Campbell, V.A. Chuyanov, et al., Proc. 22nd Fusion Energy Conference, Geneva, 2008, paper IAEA-CN-165/IT/P6-11
- [4] H.D. Pacher, A.S. Kukushkin, G.W. Pacher, et al., *J. Nucl. Mater.* **363-365** (2007) 400